JOURNAL OF Applied Polymer SCIENCE

Preparation of a poly(vinyl chloride) ultrafiltration membrane through the combination of thermally induced phase separation and non-solvent-induced phase separation

Tian-Tian Jin, Zhi-Ping Zhao, Kang-Cheng Chen
School of Chemical Engineering and the Environment, Beijing Institute of Technology, Beijing 100081, China
Correspondence to: Z.-P. Zhao (E-mail: zhaozp@bit.edu.cn)

ABSTRACT: To regulate the polymer–diluent interaction and control the viscosity of the casting solution, diphenyl ketone (DPK) and a *N,N*-dimethylacetamide/*N,N*-dimethylformamide mixture were selected as a combined diluent. Poly(vinyl chloride) (PVC) utlrafiltration membranes, which had sufficient mechanical properties for their practical applications because of their bicontinuous spongy structure, were prepared by a combined process of thermally induced phase separation and non-solvent-induced phase separation. The phase-separation mechanism was analyzed. In an air bath, the cast nascent solution immediately transformed into a transparent gel, and liquid–liquid phase separation was induced by a sudden drop in the temperature before crystallization. An ice–water bath was used to coagulate the membrane. The effects of the DPK and PVC concentrations on the membrane structures and performances were mainly investigated. The results show that an increase in the DPK content made the membrane pores change from fingerlike to spongy. Fully spongy pores formed, and the pores size decreased with increasing PVC concentration. © 2015 Wiley Periodicals, Inc. J. Appl. Polym. Sci. **2016**, *133*, 42953.

KEYWORDS: mechanical properties; membranes; poly(vinyl chloride); structure–property relations

Received 27 February 2015; accepted 16 September 2015
DOI: 10.1002/app.42953

INTRODUCTION

As a separation technology of high efficiency and low energy consumption, ultrafiltration has widely been applied in various industries. It is usually limited to membranes with pore diameters from 1 to 100 nm.[1] Membranes with high separation performances are desired and usually regarded as the goal for membrane scientists to achieve.[2] Many kinds of polymer materials have been fabricated into porous membranes for separation applications.[3] One of the research trends in the membrane field has strongly focused on new techniques for fabricating membranes with preferable structures and performances.

Phase inversion is a well-known process that is used for the preparation of porous membranes.[4–6] According to the different induction forces, phase-inversion processes can be categorized into non-solvent-induced phase separation (NIPS),[7] thermally induced phase separation (TIPS),[8] and vapor-induced phase separation.[9,10] The TIPS procedure is perhaps the most versatile and simplest membrane preparation technique.[4] Since this method was introduced by Castro and Park[8] in the late 1970s, many polymer materials have been made into microporous membranes; these include polyethylene,[11,12] polypropylene,[13] polyvinylidene fluoride (PVDF),[14,15] poly(ethylene-*co*-vinyl alcohol),[16,17] polystyrene,[18] and poly(methyl methacrylate).[19] In the process of membrane preparation via TIPS, a polymer is dissolved in a diluent at high temperature, and then, the homogeneous polymer solution is cooled to induce phase separation.[20] In this process, liquid–liquid phase separation or solid–liquid phase separation occurs; this depends on the polymer–diluent interaction, composition, and thermal driving force.[21] During liquid–liquid phase separation, a polymer-rich continuous phase and a polymer-lean droplet occur; then, a cellular, lacy, or bicontinuous structure is formed after the diluent is removed by solvent extraction, and the final membrane shows excellent mechanical properties, a high porosity, and water permeability.[12] A leaf is produced or a spherulitic structure is usually formed in solid–liquid phase separation as the polymer solidifies or crystallizes before liquid–liquid phase separation, and the resulting membranes present low breaking stress and elastic moduli.[12] That is, the phase-separation behavior has an important impact on the final morphology and properties of the membrane in the TIPS process, and one can control the path of phase separation by choosing suitable diluents, appropriate polymer concentrations, and other factors that affect the morphology of the membranes.[22]

Poly(vinyl chloride) (PVC) is a cheap material compared with common membrane materials such as polystyrene, polyacrylonitrile (PAN), polyether sulfone (PES), and PVDF. Within the temperatures range 288–313 K, PVC displays its most usable

Table I. Summary of the Progress in the PVC Membrane Development

Source	Method	Solvent/additive	Membrane structure	Purpose	Application
Fan *et al.*[24]	NIPS	DMAc/polyvinyl formal	Fingerlike pores	Improve antifouling with additives	Water treatment
Hirose *et al.*[7]	NIPS	DMF	Fingerlike pores	Affect the leaching time and gelation bath	Immobilization of enzymes
Bodzek and Konieczny[23]	NIPS	DMF	Fingerlike pores	Effect of the polymer molecule	Water treatment
Okuno *et al.*[25]	NIPS	DMF/DMAc/tetrahydrofuran/water/methanol/ethanol/*n*-propanol	Fingerlike pores	Affect the additive, polymerization, and polymer concentration	Pervaporation
Xu and Xu[26]	NIPS	DMAc/PEG/poly(vinyl pyrrolidone)	Fingerlike pores	Regulate and control the membrane structure with additives	Water treatment

PEG, poly(ethylene glycol).

properties; it deteriorates slightly (particularly the mechanical properties) as the glass-transition temperature is approached (348–316 K).[23] It is stiff and has excellent physical and chemical properties, such as resistances to acids, alkalis, chlorine, and solvents.[24] So, close attention has been paid in the membrane field to PVC as a promising material for the fabrication ultrafiltration membranes and microfiltration membranes. However, because it is limited by the thermal stability, the preparation process of PVC membranes is usually NIPS, as presented in Table I. These reported preparation processes are all NIPS processes, and the membranes all had fingerlike structures. As a result, the mechanical strength was not good enough for further applications, such as water purification, sewage treatment, gray water recycling, and beverage, sugar, and wine treatments. One way to solve this issue is to develop multichannel membranes, but this comes at a cost of flux loss.

In general, because of the weakness in mechanical properties of membranes prepared via the NIPS process, the TIPS process seems to be a possible alternative. With regard to PVC materials, however, the temperature of the casting polymer solution cannot exceed 130°C because of its thermal stability. Below this moderate temperature, the solubility of PVC in a diluent with the TIPS method is generally too low to endow the resulting membranes with sufficiently mechanical strength. It is not possible to increase the PVC concentration with diphenyl ketone (DPK) as a solediluent in the TIPS process.

In this study, we selected DPK and a *N,N*-dimethylacetamide (DMAc)/*N,N*-dimethylformamide (DMF) mixture at a certain ratio as a combined diluent to prepare PVC porous membranes via a combined process of TIPS and NIPS. Poly(ethylene glycol) 600 (PEG 600) was also used as an additive because of its solubility in the casting solution, and we chose an extraction agent (ethanol). We used PEG 600 for its film-forming properties as well, as reported by Xu *et al.*[26] We investigated in detail the effects of the DPK content and polymer concentration on the morphology, pore structure, mechanical properties, permeability (flux), and rejection performance of the obtained membranes. The main aim of this study was to develop PVC ultrafiltration membranes with bicontinuous structures to improve the mechanical properties. The phase-separation mechanism for the formation of the nascent membranes from the combined TIPS and NIPS processes was also explored.

EXPERIMENTAL

Materials

PVC (degree of polymerization (DP) = 2500) was purchased from Hangzhou Electrochemical Group Co., Ltd. It began to decompose at 130–140°C; this was measured by the mass loss on a Seiko thermogravimetry-differential thermal (TG–DTA) instrument.

DPK, DMF, DMAc, ethanol, and PEG 600 were used as analytical reagents and were purchased from Tianjin Fuchen Chemical Reagent Factory. The solubility parameters of the components used to form the membrane casting solutions are listed in Table II. Bovine serum albumin (BSA) with a molecular weight of 67 kDa was purchased from Sinopharm Chemical Reagent Co., Ltd. Ultrapure water was prepared with Aquapros ultrapure water equipment. All of the materials were used without further purification.

Membrane Preparation

The solubility parameter of DPK (22.1 $MPa^{1/2}$) was so close to that of PVC (21.4 $MPa^{1/2}$) that it was capable of dissolving PVC at an appropriate temperature. On the other hand, the melting point of DPK was 48.5°C (i.e., below this temperature, DPK was in crystal form). As a solid diluent, not only is it typically removed by solvent extraction from nascent membranes, but

Table II. Solubility Parameters of the Components Used in the Membrane Casting Solutions[27]

Chemical	PVC	DPK	DMAc	DMF	PEG
Solubility parameter ($MPa^{1/2}$)	21.4	22.1	22.7	24.8	—

PEG, poly(ethylene glycol).

also it can be recycled easily by solvent evaporation; this saves resources and reduces pollution.

PVC, DPK, the DMAc/DMF mixture, and PEG 600 were weighed at a certain mass ratio and mixed in a glass vessel to prepare the casting solution. The ingredients of the casting solution were denoted as *m*P(*x*D*y*M*z*A), where P, D, M, and A stand for the polymer (PVC), diluent (DPK), DMAc/DMF mixture, and additive (PEG 600), respectively, and *m, x, y,* and *z* are the corresponding weight percentages. For example, 10P(7.2D64.8M18A) means that the concentrations of the polymer (PVC), diluent (DPK), DMAc/DMF mixture, and additive (PEG 600) were 10, 7.2, 64.8, and 18 wt %, respectively.

With the properties of PEG 600 and the casting solution and the expected membrane structure, the content of PEG 600 was fixed at 17.2 wt %. This was a compromise value based on the work of others[28] who found that with increasing additive content, the viscosity of the casting solution increased and, at the same time, the membrane structure changed from fingerlike pores to spongy pores.

The casting solutions were prepared by the dissolution of PVC powders in the combined diluents under continuous agitation at 100°C for 2 h. We allowed them to stand for 30 min at 100°C to degas. The clear homogeneous solution was cast onto a clean, smooth glass plate that was preheated to 110°C. The thickness of the nascent membranes was controlled at a uniform size of 330 μm by the placement of two layers of double-sided adhesive tape on both edges of the glass plate. Then, the glass plate with the cast membrane solution was naturally cooled in air or immersed in an ice–water coagulation bath (quenching medium) until the phase-separation process was completely accomplished. After that, the membrane was kept in ethanol for 48 h to extract the rest of the diluents. When the membranes were completely dried in air, their properties were tested.

Scanning Electron Microscopy (SEM) Observation

Field emission scanning electron microscopy (FESEM; JSM7401, LEI) was used to investigate the morphologies of the membranes. A dry PVC membrane was frozen and fractured in liquid nitrogen to measure the cross section. After the samples were sputter-coated with gold with an ion sputterer (JFC-1100), the cross section and surfaces were imaged by FESEM at an acceleration voltage of 3.0 kV.

Pore Size Distribution

The pore size distribution of the membranes was measured by a capillary flow aperture instrument (Porolux1000, Quantachrome, United States). The membrane samples were prepared as discs with diameters of 25 mm. Before the measurement, the membrane was fully infiltrated with a Porofil liquid (Perfluoroether, surface tension = 19 mN/m).

Porosity Determination

The porosity is defined as the volume of pores divided by the total volume of the membrane. The dry membrane sample (20 × 20 mm^2) was first weighed and was then immersed in ethanol and ethanol–water mixtures at different proportions (3:1, 2:2, and 1:3) and pure water for about 24 h. Finally, the wet membrane with pores fully filled with water was weighed in a weighing bottle as soon as the water on the external surface of membrane was wiped with a piece of dry filter paper. The porosity was calculated by the following equation and averaged[20]:

$$\varepsilon = \frac{(w_0 - w_1)/\rho_{water}}{(w_0 - w_1)/\rho_{water}/\rho_{PVC}} \times 100\% \quad (1)$$

where ε is the porosity of membrane, w_0 is the weight of the wet PVC membrane, w_1 is the weight of the dry PVC membrane, and ρ_{water} (1.0 g/cm^3) and ρ_{PVC} (1.4 g/cm^3)[29] are the densities of water and PVC, respectively. The average of at least three parallel experimental results is presented.

Table III. Thickness of the Membranes

Membrane	Thickness (μm)	Membrane	Thickness (μm)
0	100	6	134
1	180	8	135
2	162	9	123
3	128	10	134
4	111	11	122
5	100	12	114

Tensile Tests

The tensile strengths of the PVC membranes were measured with a tensile test instrument (RGM-4000, Shenzhen REGER Instrument Co., Ltd., China). The test was carried out at a strain rate of 2 mm/min at room temperature. The membrane samples were cut into a rectangular shape (35 × 10 mm^2). The thickness was measured exactly with a thickness gauge (CH-1-S/ST, Shanghai Liuling Instrument Plant, China), and it is listed in Table III. The data of the tensile strength were determined according to the engineering stress–strain curve. The average of at least three parallel results is reported.

Water Permeation and Retention Measurements

The water permeation was measured with an experimental device that we made. The membrane sample, with a 10.2-cm^2 effective area, was first installed into the permeation cell and compacted by the filtration of ultrapure water at 0.1 MPa and 25°C for 10 min; then, the weight of pure water was recorded by an electronic balance every 30 s for 5 min. The pure water flux (J) was calculated by the following equation, and the values were averaged:

$$J = \frac{V}{St} \quad (2)$$

where V, S, and t represent the volume of permeated water (L), membrane area (m^2), and permeation time (h), respectively. For each sample, three membranes were measured in parallel, and the average water flux was reported.

Rejection measurements were carried out with BSA as a model protein. A series of BSA aqueous solutions with different known concentrations were tested for absorbance with an ultraviolet–visible spectrophotometer at 278 nm, and a calibration curve of the absorbance against the BSA concentration was constructed. A

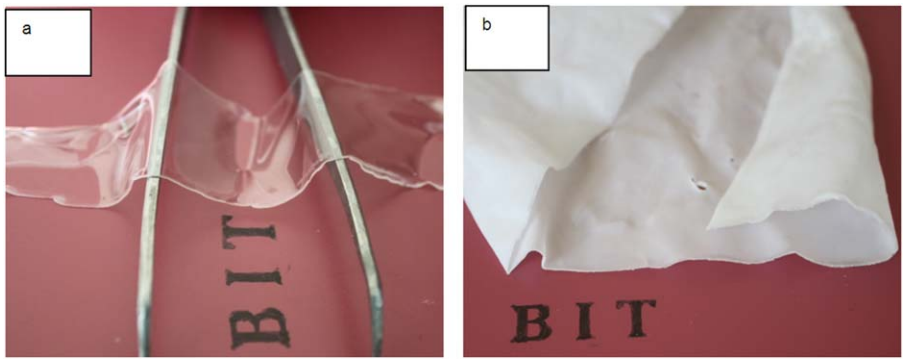

Figure 1. Changes in the morphology of the membranes coagulated by natural cooling under airtight conditions. The nascent membrane was (a) cooled for 10 min and (b) crystallized for 24 h. The PVC and DPK contents were 16 and 41.3 wt %, respectively. [Color figure can be viewed in the online issue, which is available at wileyonlinelibrary.com.]

0.1 g/L BSA solution was used as the feed solution for the rejection measurements. The test of protein retention of each membrane was conducted after the pure water flux measurement. The concentration of BSA in the permeate solution was obtained from the calibration curve. The protein rejection was calculated by the following equation, and the values were averaged:

$$R=\left(1-\frac{C_p}{C_b}\right)\times 100\% \quad (3)$$

where R, C_b, and C_p represent the protein rejection ratio of the membrane (%), the concentration of the feed solution (g/L), and the concentration of the permeate solution (g/L), respectively. For each sample, three membranes were measured in parallel, and the average protein rejection is reported.

RESULTS AND DISCUSSION

Phase Separation

Membrane Prepared via Natural Cooling. An air bath at room temperature was first used to observe the effect of the temperature on the formation of the nascent membrane. The nascent membrane prepared from a 16 wt % polymer and a DPK content of 41.3 wt % was transparent and soft (i.e., the casting solution became a gel) after it was cooled naturally (slow cooling) for several minutes [Figure 1(a)]. Crystallization occurred

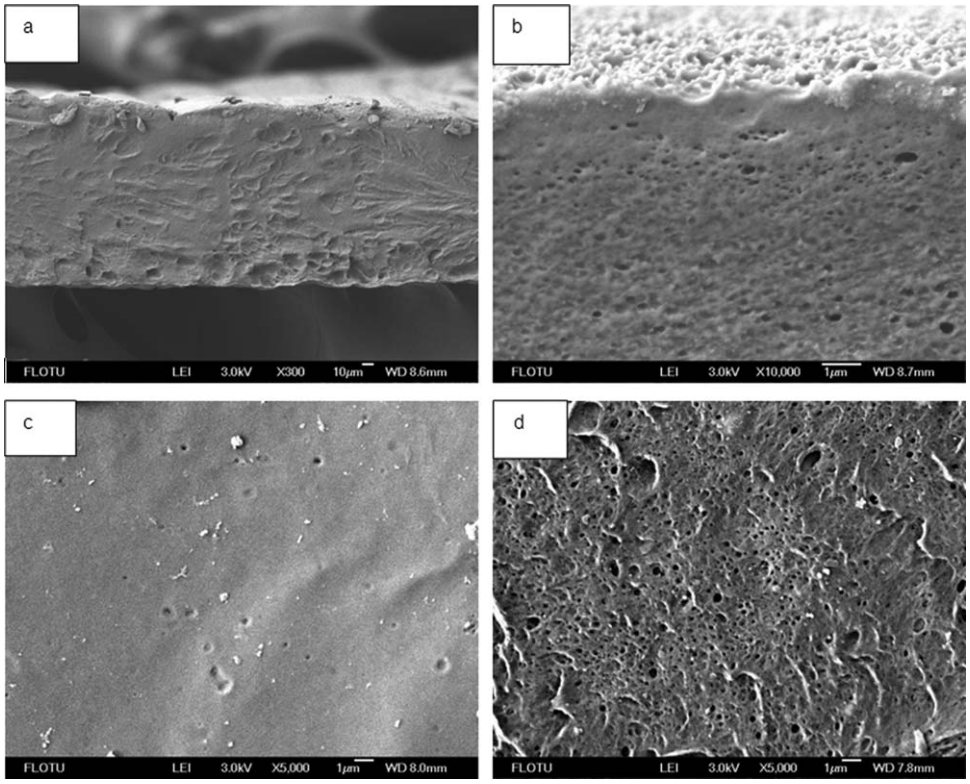

Figure 2. SEM micrographs of the nascent membrane extracted after crystallization for 12 h (coagulated by natural cooling under airtight conditions): (a) cross section (300×), (b) cross section (10,000×), (c) air surface (5000×), and (d) glass surface (5000×). The PVC and DPK contents were 16 and 41.3 wt %, respectively.

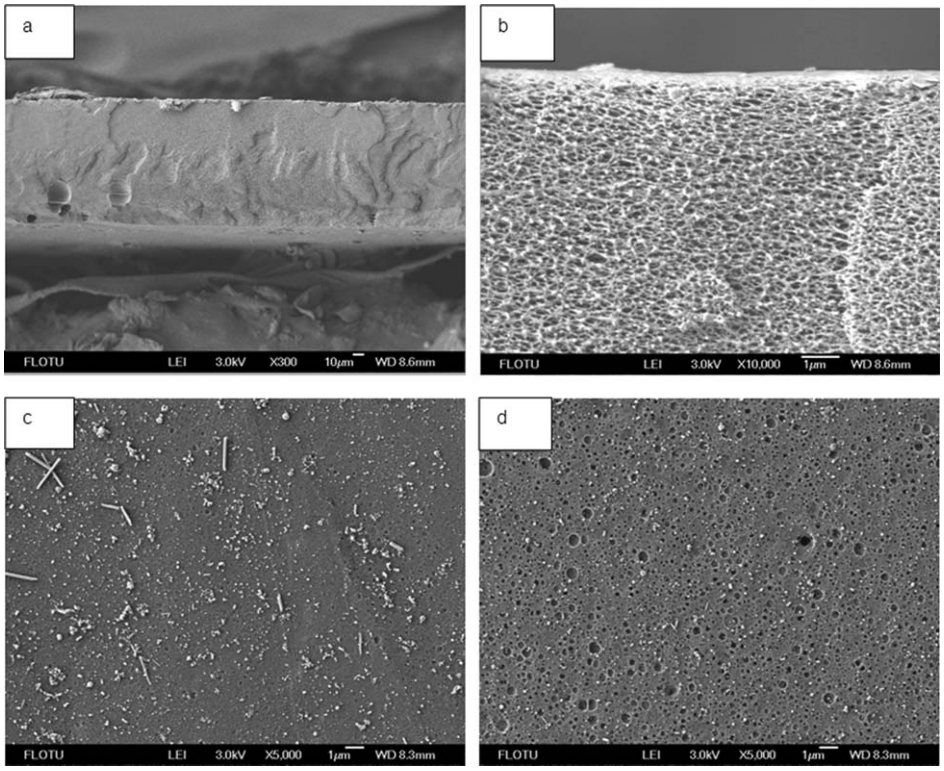

Figure 3. SEM micrographs of the extracted membrane coagulated in an ice–water bath: (a) cross section (300×), (b) cross section (10,000×), (c) air surface (5000×), and (d) glass surface (5000×). The PVC and DPK contents were 16 and 41.3 wt %, respectively.

during sequential cooling [Figure 1(b)], but the rate was very slow; it took 12 h. During this period, the membrane gradually solidified and formed finally. This was a pure cooling process, and the drop in the temperature was the only driving force for phase separation.

Figure 1 shows SEM micrographs of the previous membrane after the diluents were extracted with ethanol and after natural cooling under airtight conditions for 12 h. Net-rich and spherulitic morphologies existed together. Although no other evidence, at present, was given for the structures shown in Figure 2, it is appropriate to speculate on the membrane formation mechanism as follows. The casting solution first underwent liquid–liquid phase separation with subsequent polymer gelation before solid–liquid phase separation (mainly, the crystallization of DPK) took place. As the temperature decreased and the thermal energy was removed, the intensity of the PVC–DPK interactions decreased. As a result, the PVC molecules and DPK molecules retracted from each other, and liquid–liquid phase separation first occurred. After this, the molecules of DPK, DMAc, and DMF in the polymer gel and shown in Figure 1(a) were still capable of diffusion and transference. Solid–liquid phase separation proceeded via the nucleation and growth of DPK as did further enrichment in the liquid of DMF rather than DMAc being dispersed in the polymer gel system with the subsequent solidification of PVC. The solubility parameters presented in Table II indicated that PVC/DMAc was a miscible system whose compatibility was better than that of PVC/DMF. As the temperature decreased, the intensity of the interaction decreased; that is, the PVC/DMF system became slightly less compatible. Consequently, for a given polymer, phase separation could be shifted to a higher temperature at a fixed polymer concentration through the selection of a less compatible diluent.[30] This was main reason why the DMF was selected as one component of the combined diluents.

Because of the gelation of the casting solution, we tried in vain to measure the cloud point[29] curves and binodals with a thermosoptical microscope. As described previously, PVC had good compatibility with the DMAc/DMF mixture. Upon early cooling, the PVC molecules only retracted from the DPK molecules rather than from the DMAc and DMF molecules. Of course, this system underwent liquid–liquid phase separation but did not exhibit a cloud point. In fact, phase diagrams for polymeric systems are sparsely reported, and phase diagrams will need to be measured for this polymer-combined diluent system.

Furthermore, although the extracted membrane had a net-rich structure, a spherulitic morphology in the cross section, and many pores on the bottom surface in contact with the glass plate, no water permeation was observed. This was attributed to the dense structure of the top surface [Figure 2(c)] in contact with the air. This resulted from the evaporation of large amounts of the DMAc/DMF mixture during cooling in air.

Coagulation in an Ice–Water Bath. Figure 3 shows the whole and partial cross sections of the membrane that was prepared from the same casting solution, and the membrane is shown in Figures 1 and 2 with ice–water as the coagulation bath.

The extracted membrane had a mainly bicontinuous structure. In this preparation process, both the mass transfer (mutual

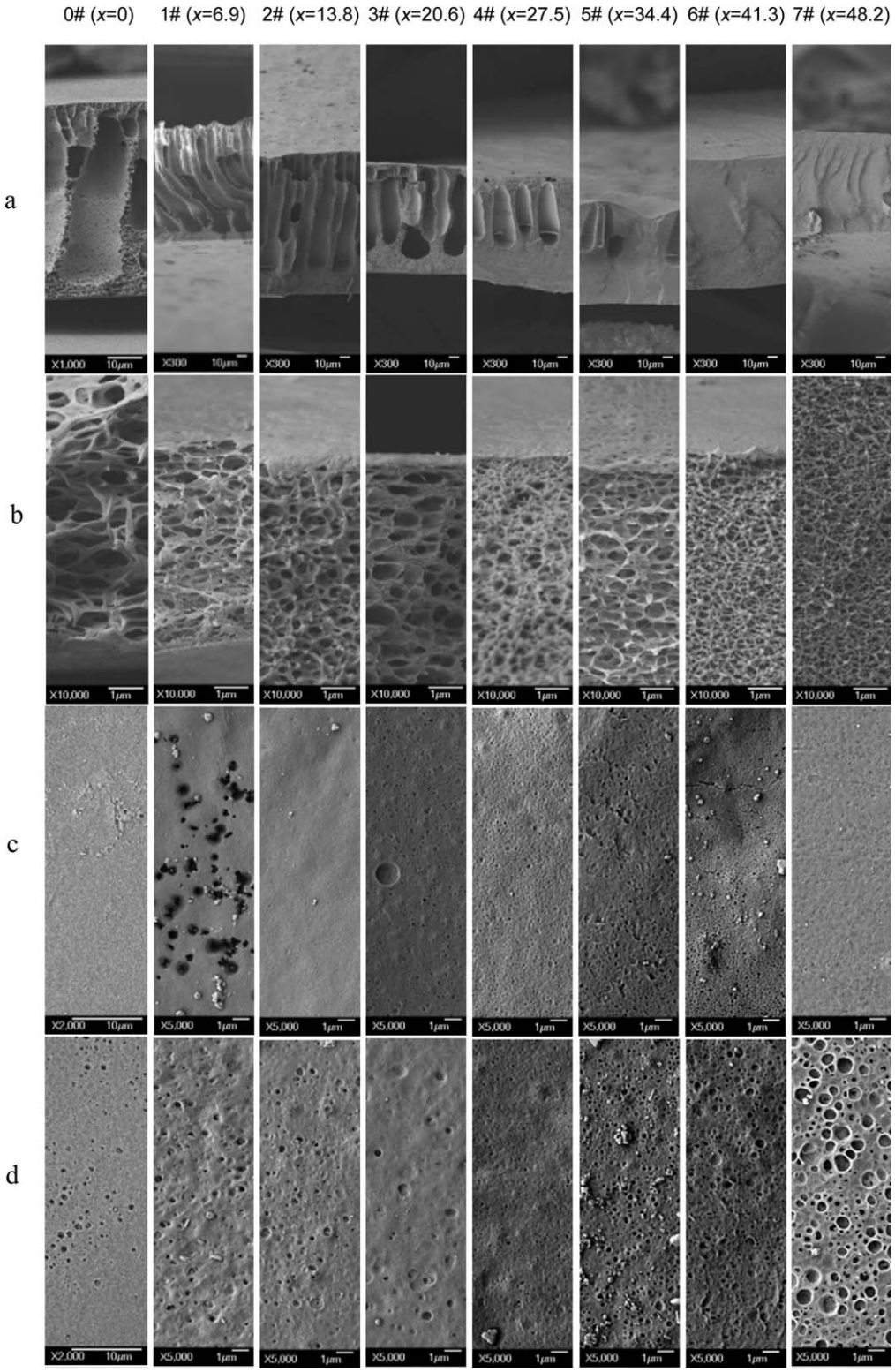

Figure 4. SEM micrographs showing the effect of the DPK content on the membrane structure: (a) cross section (300×), (b) in cross section (10,000×), (c) air surface (5000×), and (d) glass surface (5000×). The PVC content was 14 wt % except for 0 (12 wt %).

diffusion between the DMAc/DMF mixture and water) and heat transfer (cooling) proceeded in ice–water bath. The water that diffused into the nascent membrane induced the coagulation of PVC and the crystallization of DPK. This mass transfer mainly caused a NIPS process. At the same time, the existence of a temperature gradient between the casting solution and ice–water weakened the polymer–diluent interaction (with a greater interaction parameter); this caused a liquid–liquid TIPS process at a

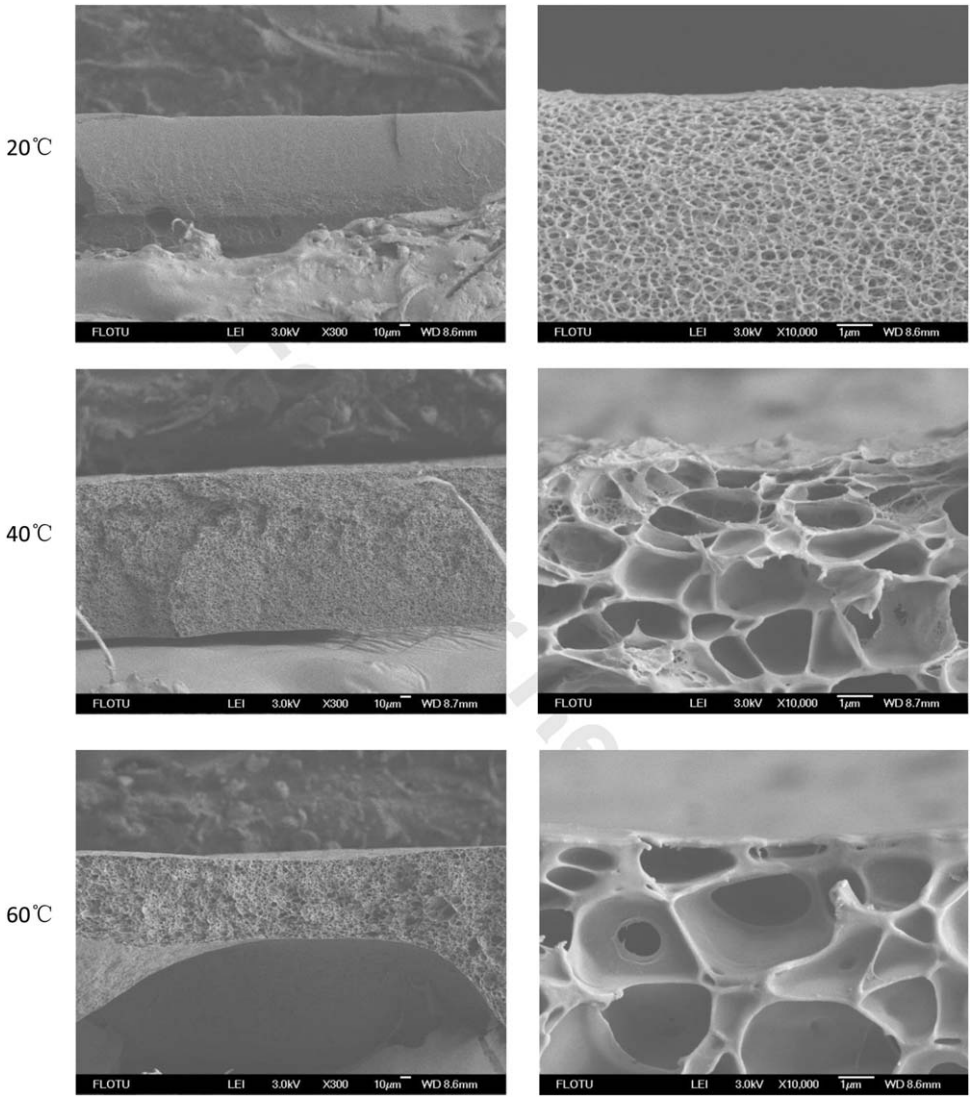

Figure 5. SEM micrographs showing the membrane structure obtained at different coagulation bath temperatures: (a) cross section (300×) and (b) cross section (10,000×). The PVC content was 14 wt %.

low initial PVC concentration. Furthermore, the temperature decrease of the casting solution not only accelerated the crystallization of DPK but also made the viscosity of the cast increase and hindered the speed of mass transfer. Therefore, NIPS was conducted in a delayed way. Thus, phase separation combining TIPS and NIPS occurred; this was driven from nucleation growth and a spinodal decomposition mechanism, which led to not only a pretty spongy structure in the cross section [Figure 3(a,b)] but also many pores in both surfaces [Figure 3(c,d)].

SEM Analysis of the Effects of the Preparation Conditions on the Morphology

Effects of the DPK Content. Figure 4 shows the cross section and surface morphology of the PVC membranes prepared with various contents of DPK in the combined diluent at a constant 14 wt % PVC and 17.2 wt % PEG 600 content. Membrane samples were prepared according to the following proportion of DPK and the DMAc/DMF mixture in the casting solution:

$$D : M = x(68.8 - x) \quad (4)$$

where x is the percentage of DPK, and the samples were numbered as 0 ($x = 0$), 1 ($x = 6.9$), 2 ($x = 13.8$), 3 ($x = 20.6$), 4 ($x = 27.5$), 5 ($x = 34.4$), 6 ($x = 41.3$) and 7 ($x = 48.2$), respectively.

The differences in the morphology were obvious in the SEM micrographs. With increasing DPK content, the cross-sectional morphologies of the membranes varied from fingerlike to uniformly spongelike. The reason was that the DMAc/DMF mixture was water-soluble and the coagulation bath was ice–water. The smaller the content of DPK was, the lower the viscosity of the casting solution was; this was due to a higher content of DMAc/DMF mixed solvents. Then, the mutual diffusion speed between solvents (DMAc/DMF mixture) and nonsolvent (water) was faster when the cast membrane solution was first immersed into the coagulation bath. Meanwhile, the concentration gradient of nonsolvent from the interface between the membrane and coagulation bath to the casting solution bulk was greater. So, the membrane formation was dominated by NIPS rather than TIPS, and an instantaneous phase separation occurred.

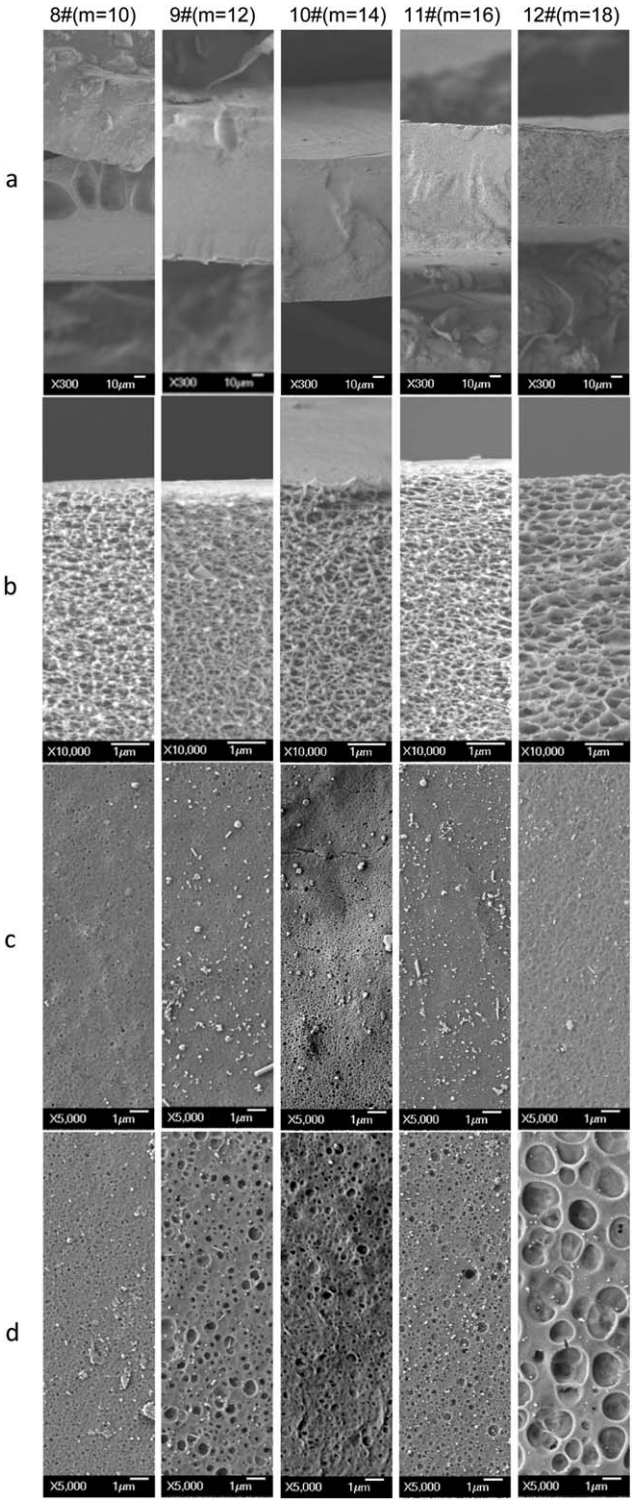

Figure 6. SEM micrographs exhibiting the effect of the PVC content on the membrane structure: (a) cross section (300×), (b) cross section (10,000×), (c) air surface (5000×), and (d) glass surface (5000×). The DPK content was 41.3 wt %.

It is worth noting that the melting temperature of DPK was 48.5°C; this was not much lower than the initial temperature (ca. 100°C) of the casting solution. Therefore, the nonsolvation behavior of DPK in the casting solution was sensitive to the decrease in the temperature as the thermal energy of the casting solution was removed. When the content of DPK reached 41.3 wt % and higher, due to the two facts—(1) the nonsolvation of DPK was sensitive to the drop in temperature, and (2) the increased viscosity of the casting solution limited the mutual diffusion between the DMAc/DMF mixture and water to some extent and the concentration gradient of nonsolvent was gentle—there was a delayed phase separation in the interior of the casting solution by TIPS with NIPS forming a spongy pore structure. Therefore, the cross section of the membrane changed from a typical fingerlike structure to a uniform spongelike structure with increasing DPK content, and the skin layer changed from dense to a relatively loose structure. The pictures of the cross section also showed a gradual transition from fingerlike pores near the air-side surface to spongy pores in the glass-side surface when the DPK content was below 41.3 wt %. The area with spongy pores in the cross section was gradually extended until the fingerlike pores fully disappeared with increasing DPK content. In addition, the DPK hindered the speed of mass transfer; another reason was that the intimate contact of the nascent membrane with glass plates also hindered the exchange between the DMAc/DMF mixture and water. This further resulted in a delayed phase separation near the glass-side surface.

It is necessary to point out that if the percentage of DPK in the combined diluent was continuously increased over 48.2 wt % (x), the viscosity of the casting solution would be too high to be cast below the thermal degradation temperature of PVC. Therefore, the DPK percentage of 41.3 wt % (x) was selected to prepare the membranes examined in this study.

Figure 5 presents the membranes prepared in coagulation baths with different temperatures, including 20, 40, and 60°C, under the same casting solution conditions as sample 6. When the temperature of the coagulation bath was increased to 60°C, the membrane structure still retained a uniform spongelike appearance because of the high DPK content. At higher temperatures, the difference in the temperature between that of the cast solution and that of the coagulation bath decreased. This diminished TIPS produced a phase-separation effect. At the same time, the mutual diffusion speed between solvents (DMAc/DMF mixture) and nonsolvent (water) was enhanced. There was a trade-off between TIPS and NIPS. The membrane became more spongelike in structure.

Effect of the PVC Content. The effect of the PVC concentration on the membrane structure was investigated through the choice of the diluent constitution of 6. The content of PVC varied from 10 to 18 wt %. Samples were prepared according to the ingredient proportion of the casting solution as expressed by the following equation:

Table IV. Most Probable Pore Size of Membranes Prepared with Different PVC Contents

m (wt %)	10	12	14	16	18
Most probable pore size (nm)	38.5	36.6	35.4	29.7	26.2

The condition was a constant DPK content of 41.3 wt %.

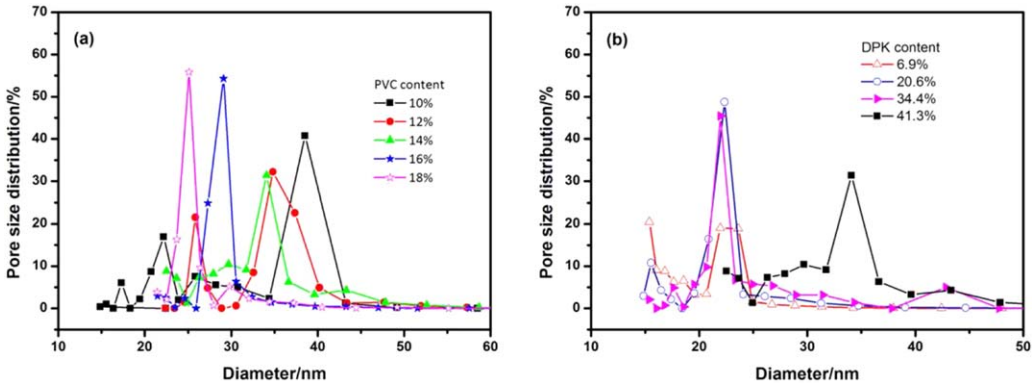

Figure 7. Variation of the pore size with the (a) PVC and (b) DPK content. [Color figure can be viewed in the online issue, which is available at wileyonlinelibrary.com.]

$$P : D : M : A = m : 0.48(100-m) : 0.32(100-m) : 0.2(100-m) \quad (5)$$

where m is the percentage of PVC, and the samples were numbered as 8 ($m = 10$), 9 ($m = 12$), 10 ($m = 14$), 11 ($m = 16$), and 12 ($m = 18$), respectively. The cross-sectional and surface morphologies of all of the membranes are presented in Figure 6. The membranes showed a few large cavities in the cross section near the air-side surface when the PVC concentration was lower than 14 wt %; when the concentration was 14 wt % and higher, the whole cross-sectional morphology presented a uniform sponginess. The reason was that the increasing polymer concentration boosted the viscosity of the casting solution. The lower the concentration and viscosity of the casting solution were, the greater the speed of mass transfer was. So, instantaneous NIPS dominated the phase separation. When the concentration of the polymer was 14 wt % and greater, the viscosity of the casting solution increased, and the NIPS process was so seriously inhibited that TIPS and delayed NIPS acted together to form spongy pores. Therefore, the membrane morphology changed fully from typical fingerlike pores and relative loose skin to a uniform spongelike appearance and dense skin.

Pore Size Distribution and Porosity

The most probable pore size and pore size distribution of the membranes prepared with different polymers or DPK concentrations were investigated, and the results are presented in Table IV and Figure 7, respectively. The most probable pore size of the membranes decreased from 39 to 26 nm with increasing polymer content, and the pore size distribution became narrower in Figure 7(a). These regular variations were similar to the other reported results.[20,31] Wu *et al.*[20] prepared a PAN membrane via TIPS and studied the effect of the polymer content on the pore size distribution. The pore size got smaller, and the distribution got narrower with increasing PAN concentration. Hou *et al.*[31] also reported this kind of change in the pore size while preparing PVDF flat-sheet membranes via NIPS. Furthermore, the areas surrounded by the curve of the pore size distribution in Figure 7(a) revealed that the pore number/density decreased with increasing PVC content.

The effect of the DPK content on the pore size distribution is shown in Figure 7(b). At the same PVC concentration (14 wt %), the most probable pore size of the air-side layer changed little when the DPK content increased from 6.3 to 34.4 wt %. When the DPK content increased to 41.3 wt %, the pore size jumped to 35 nm. We also found that the area of the pore size curve against the diameter increased with DPK content; this suggested that the pore density on the air surface increased.

Figure 8 presents the porosities of the membranes, which gently decreased with increasing DPK content in combined diluent at a certain PVC concentration. This phenomenon could be explained from the microstructure of the membranes shown in Figure 4. When the DPK content was 34.4 wt % (x) or less, there were many fingerlike macropores; when it was higher than 34.4 wt %, the structure was uniformly spongelike.

The porosities had a more obvious trend, dropping with increasing PVC content (Figure 9). This could also be illustrated from the structure of the membranes, as shown in Figure 6. The decrease in the porosity was mainly related to the decrease in the volume of the combined diluent. On the other hand, the increased viscosity of the casting solution limited the movement of the polymer molecules during phase separation. At this moment, membrane formation was in a more delayed phase-separation process.

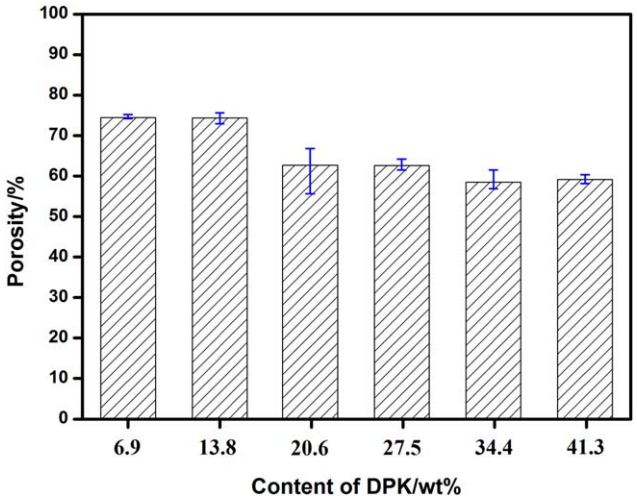

Figure 8. Variation of the porosity of the PVC membranes with the DPK content at a constant PVC concentration of 14 wt %. [Color figure can be viewed in the online issue, which is available at wileyonlinelibrary.com.]

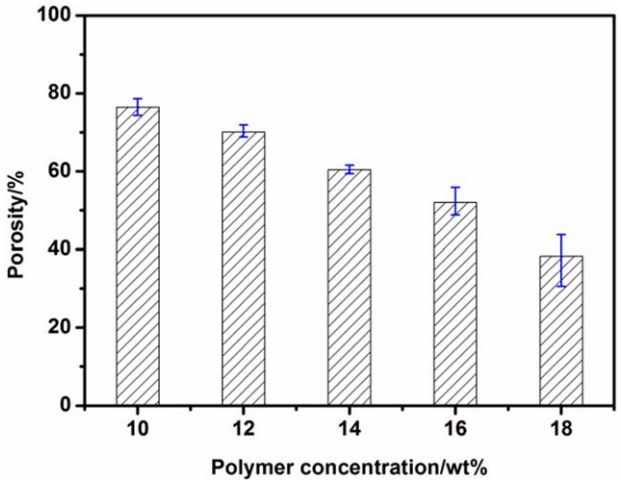

Figure 9. Variation of the porosity of the PVC membranes with the PVC content at a constant DPK content of 41.3 wt %. [Color figure can be viewed in the online issue, which is available at wileyonlinelibrary.com.]

Tensile Strength of the Membranes

Effect of the DPK Content on the Tensile Strength. The engineering stress–strain analysis results of the membranes fabricated from different DPK contents are displayed in Figure 10, where the curves are assigned to samples 1–6, respectively. The yield stress increased with increasing DPK content. The tensile strength of each membrane is shown in Figure 11. With increasing DPK content to 41.3 wt %, the corresponding tensile strength increased from 4.8 to 8.5 MPa. Importantly, when the PVC content was 12 wt %, the tensile strength increased considerably by 145% because of the increase in spongelike structures compared to that of membrane 0, which had a full fingerlike structure prepared via a pure NIPS process with a casting solution with DMF/DMAc as the solvents.

Effect of the PVC Concentration on the Tensile Strength. The engineering stress–strain curves of membranes fabricated from different PVC contents are displayed in Figure 12, in which the

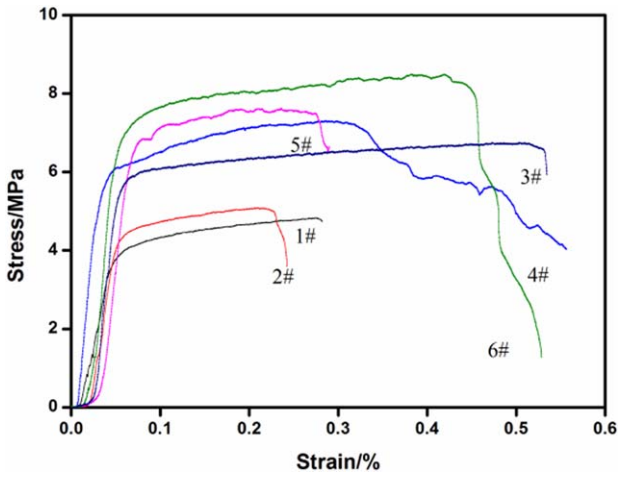

Figure 10. Variation of the engineering stress–strain curve of the PVC membranes with the DPK content at a constant PVC concentration. [Color figure can be viewed in the online issue, which is available at wileyonlinelibrary.com.]

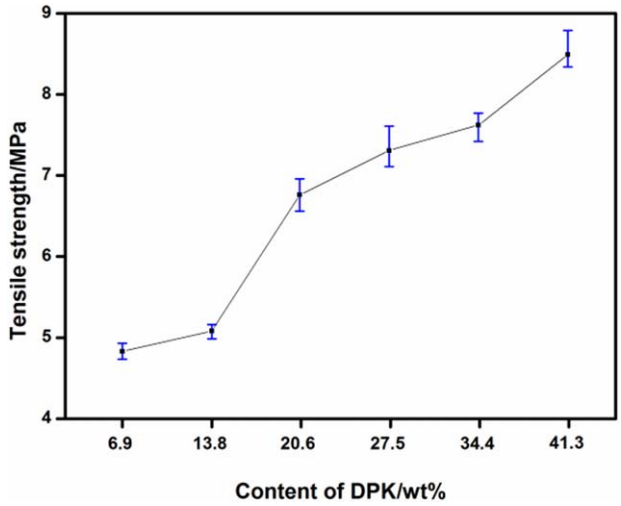

Figure 11. Variation of the tensile strength of the PVC membranes with the DPK content at a constant PVC concentration of 14 wt %. [Color figure can be viewed in the online issue, which is available at wileyonlinelibrary.com.]

curves are assigned to the membrane samples 8–12, respectively. The yield stress and tensile strength both increased with increasing PVC content. The tensile strength is shown in Figure 13. The tensile strength was varied from 4.4 to 11.1 MPa and increased by 149% when the PVC content was increased from 10 to 18 wt %. This phenomenon was explained by the microstructure of the membranes. When PVC content was 14 wt % or less, the membranes had many fingerlike macropores, which decreased the fracture force needed when they were stretched; when the PVC content was greater than 14 wt %, the membranes showed were a uniform spongelike material, which became more compacted with increasing PVC content.

Permeation Properties

In Figure 14, the pure water flux and rejection of BSA solution for the membranes prepared with different DPK contents under

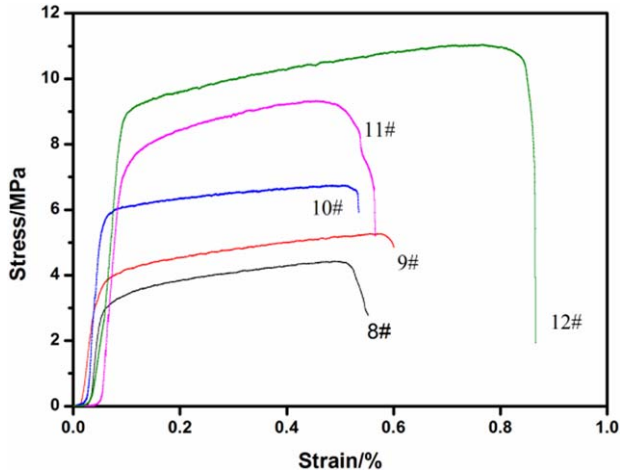

Figure 12. Variation of the engineering stress–strain curve with the PVC content at a constant DPK content 41.3 wt %. [Color figure can be viewed in the online issue, which is available at wileyonlinelibrary.com.]

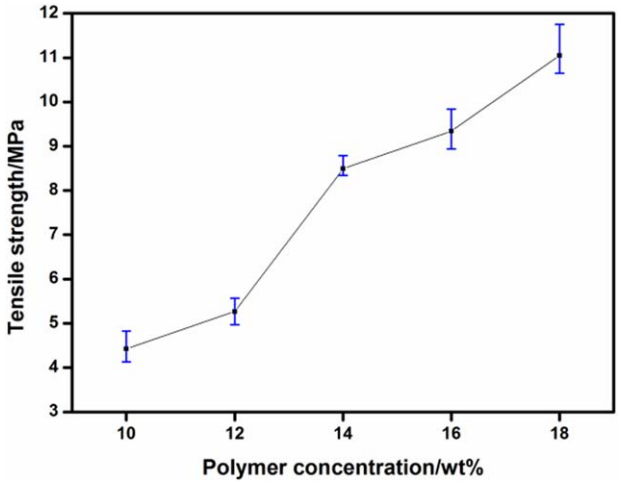

Figure 13. Variation of the tensile strength of the PVC membranes with the PVC content at a constant DPK content of 41.3 wt %. [Color figure can be viewed in the online issue, which is available at wileyonlinelibrary.com.]

the same PVC concentration of 14 wt % are presented. The figure shows that the high water flux generally correspond with low rejection. The pure water flux increased from 2.4 to 23.6 L m^{-2} h^{-1} with an increase in the DPK content from 6.9 to 41.3 wt %, but there was no obvious decrease in the BSA rejection. Figure 8 shows that only a small change in the porosity was detected. The reason for the increase in the pure water flux was due mainly to the air surface of the membrane having an increased pore density [see Figure 7(b)], so it became looser as a result of the less volatile DMAc/DMF mixture in the casting solution. Thus, the effect of the thickness of the resulting membranes on the permeability could be ignored when the water flux was relatively low. At this time, the water permeation resistance mainly stemmed from the dense top layer. On the other hand, some of the BSA molecules were generally aggregated in solution rather than dispersed fully. As a result, the increase in

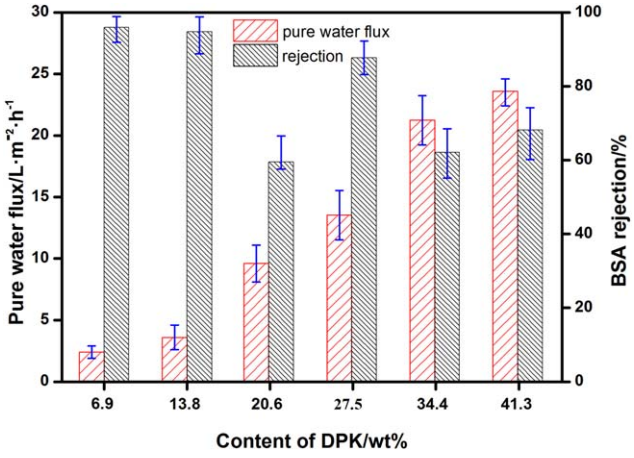

Figure 14. Variation of the water flux and BSA rejection of the PVC membranes with the DPK content at a constant PVC concentration of 14 wt %. [Color figure can be viewed in the online issue, which is available at wileyonlinelibrary.com.]

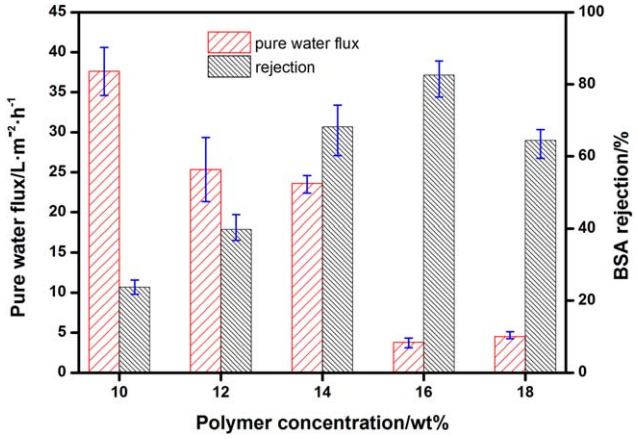

Figure 15. Variation of the water flux and BSA rejection of the PVC membranes with the PVC concentration at a constant DPK content of 41.3 wt %. [Color figure can be viewed in the online issue, which is available at wileyonlinelibrary.com.]

the DKP content did not bring about an obvious downward trend in the BSA rejection.

The pure water flux and rejection of the BSA solution were also tested for the membranes fabricated with different PVC contents under the same combined diluent (DPK content = 41.3 wt %). Figure 15 shows that the flux decreased with increasing PVC concentration, and there was a tendency for the rejection to increase. These effects of the PVC concentration on the permeation and rejection resulted from decreases in the pore size (Figure 7) and porosity (Figure 9) of the membranes, through which the water permeated with greater resistance.

With regard to the 16 wt % membrane having a higher rejection than the 18 wt % membrane, it is possible that gel formation was more sensitive to a decrease in temperature at the higher polymer concentrations, and a few defects were more readily formed during membrane casting because of gelation. At present, this is speculative and requires further investigation.

CONCLUSIONS

PVC ultrafiltration membranes with spongelike/bicontinuous structures were prepared via a combined process of TIPS and NIPS. We selected DPK and the DMAc/DMF mixture as combined diluents to regulate the polymer–diluent interaction and control the viscosity of the casting solution and PEG 600 as an additive (a porosity-making agent). The mechanism for the formation of the spongelike material of the PVC membranes was analyzed. The main points are summarized as follows.

First, in an air bath at room temperature, the nascent cast membrane solution immediately transformed into a transparent gel in 1 min, and liquid–liquid phase separation was induced before solid-phase separation (mainly, the crystallization of DPK) on further cooling.

Second, the membrane structures coagulated via an ice–water bath were significantly affected by the contents of both DPK and PVC. Under a given PVC concentration, with increasing DPK content, the membrane formation was dominated by TIPS

combined with a delayed NIPS, in which the mass transfer rates were markedly reduced because of the decrease in the DMAc/DMF mixture and the increase in the viscosity of casting solution. A delayed phase separation caused a change in the membrane morphology from fingerlike to uniformly spongelike. The membrane with a uniform spongelike morphology displayed a higher mechanical strength than the membranes with fingerlike structures. An increase in the tensile strength of the ultrafiltration membranes by at least 145% was sufficient for their use in many commercial applications. On the other hand, a few large cavities in the cross section of the membranes, as observed at a concentration of 12 wt % PVC and less than a DPK concentration of 41.3 wt %, would be detrimental to their application in critical situations.

Third, changes in the contents of DPK and PVC had different effects on the membrane separation performances. The water flux increased significantly with the content of DPK; this was mainly due to the looser structure of the air surface of the membrane, but there was no obvious decrease in the BSA rejection. With regard to the increase in the PVC concentration, decreases in the pore size and porosity helped to improve the rejection, and this was accompanied by a decrease in the flux.

Fourth, the resulting ultrafiltration membranes with 60% porosity showed an inadequate BSA retention (68%). If an aqueous solution of dextran (molecular weight distribution = 110,000) was used for filtration operations, the rejection was more than 90%. On the other hand, when they were prepared on an industrial casting machine on a production scale, the membranes were improved in performance because of a reduction in pore defect.

ACKNOWLEDGMENTS

The authors express their gratitude to Xiao-Lin Wang of Tsinghua University for valuable suggestions. They thank the National Natural Science Foundation of China for its support (contract grant number 21276024).

REFERENCES

1. Gao, W.; Liang, H.; Ma, J.; Han, M.; Chen, Z. L.; Han, Z. S.; Li, G. B. *Desalination* **2011**, *272*, 1.
2. Tsai, H. A.; Ye, Y. L.; Lee, K. R.; Huang, S. H.; Suen, M. C.; Lai, J. Y. *J. Membr. Sci.* **2011**, *368*, 254.
3. Rajabzadeh, S.; Maruyama, T.; Sotani, T.; Matsuyama, H. *Sep. Purif. Technol.* **2008**, *63*, 415.
4. Lloyd, D. R.; Kinzer, K. E.; Tseng, H. S. *J. Membr. Sci.* **1990**, *52*, 239.
5. Wang, D. L.; Li, K.; Teo, W. K. *J. Membr. Sci.* **2000**, *178*, 13.
6. Xu, Z. L.; Qusay, F. A. *J. Membr. Sci.* **2004**, *233*, 101.
7. Hirose, S.; Yasukawa, E.; Nose, T. *J. Appl. Polym. Sci.* **1981**, *26*, 1039.
8. Castro, A. J.; Park, O. U.S. Pat. 4,247,498 (**1981**).
9. Liu, W.; Zhao, Z.; Sun, L.; Wang, M. *Chin. J. Chem. Eng.* **2010**, *18*, 529.
10. Srinivasarao, M.; Collings, D.; Philips, A.; Patel, S. *Science* **2001**, *292*, 79.
11. Yoon, J.; Lesser, A. J.; McCarthy, T. J. *Macromolecules* **2009**, *42*, 8827.
12. Liu, S. J.; Zhou, C. X.; Yu, W. *J. Membr. Sci.* **2011**, *379*, 268.
13. Younesi, M.; Bahrololoom, M. E. *J. Compos. Mater.* **2010**, *45*, 513.
14. Gu, M. H.; Zhang, J.; Wang, X. L.; Ma, W. Z. *J. Appl. Polym. Sci.* **2006**, *102*, 3714.
15. Rajabzadeha, S.; Yoshimotoa, S.; Teramotoa, M.; Al-Marzouqib, M.; Matsuyama, H. *Sep. Purif. Technol.* **2009**, *69*, 210.
16. Lv, R.; Zhou, J.; Du, Q. G.; Wang, H. T.; Zhong, W. *J. Membr. Sci.* **2006**, *281*, 700.
17. Shang, M. X.; Matsuyama, H.; Teramoto, M.; Lloyd, D. R.; Kubota, N. *Polymer* **2003**, *44*, 7441.
18. Song, S. W.; Torkelson, J. M. *Macromolecules* **1994**, *27*, 6389.
19. Graham, P. D.; Pervan, A. J.; McHugh, A. J. *Macromolecules* **1997**, *30*, 1651.
20. Wu, Q. Y.; Wan, L. S.; Xu, Z. K. *J. Membr. Sci.* **2012**, *409*, 355.
21. Ji, G. L.; Zhu, L. P.; Zhu, B. K.; Zhang, C. F.; Xu, Y. Y. *J. Membr. Sci.* **2008**, *319*, 264.
22. Yang, J.; Li, D. W.; Lin, Y. K.; Wang, X. L.; Tian, F.; Wang, Z. *J. Appl. Polym. Sci.* **2008**, *110*, 341.
23. Bodzek, M.; Konieczny, K. *J. Membr. Sci.* **1991**, *61*, 131.
24. Fan, X. C.; Su, Y. L.; Zhao, X. T.; Li, Y. F.; Zhang, R. N.; Zhao, J. J.; Jiang, Z. Y.; Zhu, J. A.; Ma, Y. Y.; Liu, Y. *J. Membr. Sci.* **2014**, *464*, 100.
25. Okuno, H.; Renzo, K.; Uragami, T. *J. Membr. Sci.* **1993**, *83*, 199.
26. Xu, J.; Xu, Z. L. *J. Membr. Sci.* **2002**, *208*, 203.
27. Hansen, C. M. Hansen Solubility Parameters: A User's Handbook, 2nd ed.; CRC: Boca Raton, FL, **2007**; p 199.
28. Li, J. F.; Xu, Z. L. *J. Appl. Polym. Sci.* **2008**, *107*, 4100.
29. Brandrup, J.; Immergut, E. H. Polymer Handbook, 4th ed.; Wiley: New York, **1999**; Vol. *67*.
30. Lloyd, D. R.; Kim, S. S.; Kinzer, K. E. *J. Membr. Sci.* **1991**, *64*, 1.
31. Hou, D. Y.; Fan, H.; Jiang, Q. L.; Wang, J.; Zhang, X. H. *Sep. Purif. Technol.* **2014**, *135*, 211.